JTTEE5 15:731-738
DOI: 10.1361/105996306X146875
1059-9630/$19.00 © ASM International

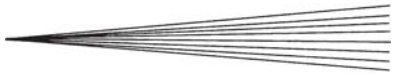

Effect of Reinforcement Size on the Scratch Resistance and Crystallinity of HVOF Sprayed Nylon-11/Ceramic Composite Coatings

S. Niezgoda, V. Gupta, R. Knight, R.A. Cairncross, and T.E. Twardowski

(Submitted February 28, 2006; Revised July 12, 2006)

The high-velocity oxyfuel (HVOF) combustion spraying of dry ball-milled nylon-11/ceramic composite powders is an effective, economical, and environmentally sound method for producing semicrystalline micron and nanoscale reinforced polymer coatings. Composite coatings reinforced with multiple scales of ceramic particulate material are expected to exhibit improved load transfer between the reinforcing phase and the matrix due to interactions between large and small ceramic particles. An important step in developing multiscale composite coatings and load transfer theory is determining the effect of reinforcement size on the distribution of the reinforcement and the properties of the composite coating.

Composite feedstock powders were produced by dry ball-milling nylon-11 together with 7, 20, and 40 nm fumed silica particles, 50 and 150 nm fumed alumina particles, and 350 nm, 1, 2, 5, 10, 20, 25, and 50 μm white calcined alumina at 10 vol.% overall ceramic phase loadings. The effectiveness of the ball-milling process as a function of reinforcement size was qualitatively evaluated by scanning electron microscopy + energy dispersive x-ray spectroscopy (SEM + EDS) microanalysis and by characterizing the behavior of the powder during HVOF spraying. The microstructures of the sprayed coatings were characterized by optical microscopy, SEM, EDS, and x-ray diffraction (XRD). The reinforcement particles were found to be concentrated at the splat boundaries in the coatings, forming a series of interconnected lamellar sheets with good three-dimensional distribution. The scratch resistance of the coatings improved consistently and logarithmically as a function of decreasing reinforcement size and compared with those of HVOF sprayed pure nylon-11.

Keywords high-velocity oxy-fuel spraying of polymers, polymer-matrix composites

1. Introduction

Polymer coatings and polymer nanocomposites are fast-growing fields in research and industry. Polymer coatings for corrosion and wear resistance are becoming ubiquitous, but can suffer from limitations such as poor scratch resistance and high permeability (Ref 1, 2). Traditionally, some of these limitations have been overcome by creating composites comprising a polymer matrix and a reinforcing material. Nanocomposite polymer research has shown that small (5 to 15 wt.%) additions of nanoscale particles can dramatically increase the yield stress, Young's modulus, and dynamic storage modulus (Ref 3-5). Recently, the correlation of materials properties with reinforcement size has become a focus in the nanocomposite literature; however, most of these studies have focused on the 1 to 100 nm range and do not extend into the micro- or mesoscale ranges, making it difficult to make direct comparisons with other technologies.

A large technical obstacle to be overcome in nanocomposite processing is achieving a uniform dispersion of the reinforcing phase (nano and micron scale) within the polymer matrix (Ref 6, 7). Traditional polymer processing methods require the use of large amounts of solvent and/or high temperatures, making polymer coating difficult to perform in the field (Ref 6). Environmental legislation and restrictions on volatile organic compounds (VOCs) point to the need for environmentally sound processing alternatives. Thermal spray is becoming recognized as an excellent solution to these limitations (Ref 8). High-velocity oxyfuel (HVOF) combustion spray offers a solventless method of producing both nano and traditional ceramic reinforced polymer composites.

A general trend of increased mechanical properties, such as Young's modulus and scratch resistance, with decreased particle size has been observed, but this effect has not been examined across both the nano and micron size scales (Ref 1). The primary aim of this work was to fully characterize the effect of reinforcement size on the properties, processing, and microstructure of ceramic particulate reinforced polymers. This was part of a broader program goal of developing improved thermally sprayed polymer ceramic multiscale coatings for industrial use in applications such as corrosion and/or wear resistance.

This article was originally published in *Building on 100 Years of Success, Proceedings of the 2006 International Thermal Spray Conference* (Seattle, WA), May 15-18, 2006, B.R. Marple, M.M. Hyland, Y.-Ch. Lau, R.S. Lima, and J. Voyer, Ed., ASM International, Materials Park, OH, 2006.

S. Niezgoda, V. Gupta, and **R. Knight,** Department of Materials Science and Engineering, Drexel University, Philadelphia, PA 19104; **R.A. Cairncross,** Department of Chemical and Biological Engineering, Drexel University, Philadelphia, PA 19104; and **T.E. Twardowski,** Twardowski Scientific 6725 Ridge Ave., Philadelphia, PA 19128. Contact e-mail: knightr@coe.drexel.edu.

2. Experimental Approach

2.1 Materials Selection

Nylon-11 (Rilsan Natural D60 ES, Arkema, King of Prussia, PA), a widely used industrial material for producing semicrystalline coatings with excellent chemical, abrasion and impact resistance, was chosen as the matrix material. Nylon-11 exhibits a large difference between melting temperature (~183 °C) and the onset of degradation (~360+ °C) that make it well suited for thermal spray deposition. The feedstock powder selected was an electrospray grade, mechanically crushed, and cryoground to a mean particle size of 60 μm by the vendor.

To isolate the effect of reinforcement particle size on the properties of the feedstock powders and coatings, ceramic reinforcements with monomodal size distributions were selected. To maximize the utility of this work to industry, it was also decided that all reinforcements selected should be "off-the-shelf" products. The particle size distribution for the reinforcement powders used was characterized using a Horiba (Kyoto, Japan) Model LA-910 laser scattering particle size analyzer and confirmed by scanning electron microscopy (SEM). White calcined alumina (Microgrit Abrasives, Westfield, MA) was chosen for the micron-scale (350 nm −50 μm) component. Commonly used in grinding and polishing applications, calcined alumina is readily available in narrow monomodal distributions across a large portion of the overall size range of interest. For the nanoscale reinforcement, fumed silica (Degussa, Piscataway, NJ: 7, 20, and 40 nm) was chosen.

2.2 Surface Treatment of Reinforcing Phase

To create a uniform surface chemistry common to all the reinforcing materials, the ceramic particles were treated with gamma-aminopropyltriethoxysilane, (Silquest A1100, G.E. Silicones, Wilton, CT). The ceramic powders were dispersed in a Silquest/toluene solution and stirred for 3 h, then dried at 120 °C to remove the solvent. The Silquest was kept at 5 wt.% concentration to maintain uniform wetting of the reinforcement surface. This treatment created a hydrophobic surface, promoting polymer/ceramic adhesion, and reduced agglomeration of the reinforcement particles (Ref 9).

2.3 Feedstock Powder Preparation

Physical blends of particles of different densities can segregate during spraying. Cospraying of the individual nylon-11 and ceramic powders can be problematic and may limit industrial application. To reduce segregation of the ceramic reinforcement and nylon-11 particles, all coatings were produced from ball-milled composite feedstock powders. Batches of ~300 g of the D60 nylon-11 were dry ball milled with 10 vol.% of ceramic reinforcement for 48 h at 75 rpm with a 900 g standard charge of alumina milling media. The composite powders were then vacuum dried at 35 °C for 24 h prior to HVOF spraying.

2.4 Coating Procedure

The coatings were produced using the HVOF process. Due to the high jet velocity, the polymer particles have very short residence times (1 to 3 ms) in the hot gas stream. It has been shown (Ref 10) that the short dwell times at temperature and high speeds result in no measurable oxidation and/or thermal degradation of the nylon-11. Other thermal spray techniques such as air plasma spray or flame spray would have longer dwell times and/or higher temperatures with consequent risks to the polymer. It was also believed that HVOF spraying offers advantages in producing semicrystalline nylon-11 coatings. The low thermal conductivity of the polymer particles and the HVOF jet work together to produce "semimolten" particles that retain much of the original crystallinity of the feedstock powder.

Table 1 HVOF process spray parameters used to deposit nylon-11/ceramic composite coatings

Parameter	Value
Powder feed rate, g/s (g/min)	0.25 (15)
Air flow rate, m^3/s (scfh)	0.5×10^{-4} (5)
Air pressure, MPa (psi)	0.42 (60)
Spray distance, mm (in.)	178 (7)
Gun surface speed, m/s (in./s)	0.23 (9.05)
Step size, mm (in.)	6.35 (¼)
Hydrogen flow rate, m^3/s (scfh)	3.7×10^{-3} (400)
Oxygen flow rate, m^3/s (scfh)	5.6×10^{-3} (600)

Coatings were produced using a Jet Kote II (Deloro Stellite, Goshen, IN) HVOF combustion spray system with internal axial powder feed. The spray nozzle was 153 mm (6 in.) in length with a bore of 8 mm (5/16 in.). Hydrogen was used as the fuel gas and argon as the carrier gas. Typical spray parameters used are listed in Table 1. Minor parameter adjustments were made, as necessary, during the coating process. Coatings were deposited onto 25.4 × 75.2 × 3 mm (1 × 3 × ⅛ in.) Al-6061 substrates. Prior to coating, all substrates were grit blasted using 1600 μm (12 grit) angular alumina and rinsed in ethanol. The substrates were preheated to 200 °C using the HVOF jet. A nominal 25 μm (0.001 in.) thick coating was first applied to the heated substrate as a bond coat. After deposition of this first layer, the substrate temperature was maintained by forced-air cooling from the rear. Higher than stoichiometric oxygen flows were used to control particle melting and increase the process stream velocity. The typical coating thickness ranged between 0.25 and 0.762 mm (0.01 and 0.03 in.).

2.5 Feedstock Powder Characterization

The morphology of the feedstock powders was characterized using an FEI (Hillsboro, OR) XL-30 field emission environmental scanning electron microscope (ESEM). The effectiveness of incorporation of the reinforcing phase after ball-milling was assessed qualitatively by energy dispersive x-ray spectroscopy (EDS) and backscattered electron (BSE) images.

2.6 Coating Characterization

The microstructures of the as-sprayed coatings were characterized by optical microscopy, ESEM secondary electron, and backscattered electron images. The coatings and substrates were sectioned, mounted in epoxy, and polished. Analysis of the distribution of the reinforcement and chemical microanalysis was performed by EDS. The crystal structure was also evaluated us-

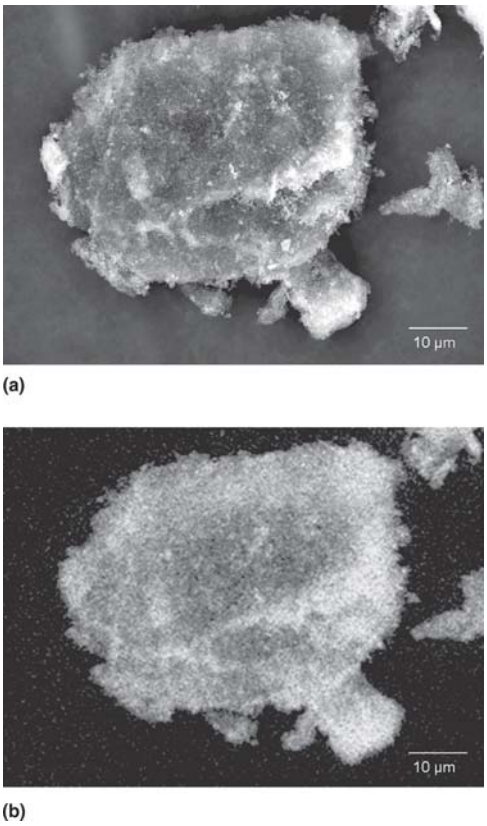

Fig. 1 SEM images of nylon-11/350 nm alumina composite particle: (a) BSE; (b) EDS dot map image showing the distribution of aluminum

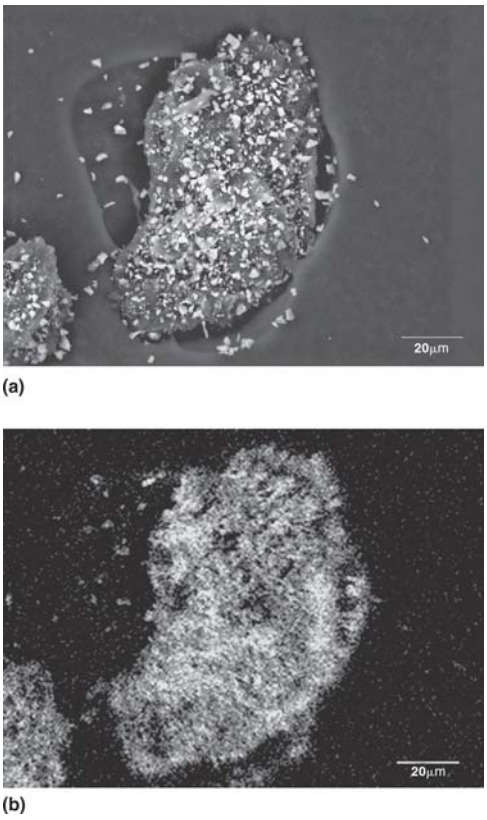

Fig. 2 SEM images of nylon-11/2 μm alumina composite particle: (a) BSE; (b) EDS dot map image showing the distribution of aluminum

ing a Siemens (now Bruker, Madison, WI) model D-500 x-ray diffractometer. Diffraction patterns were obtained by scanning over a 2-theta range of 5 to 70°.

Scratch testing was performed using a BYK Gardner (Columbia, MD) SG-8101 balance beam scrape adhesion and mar tester, according to ASTM D 5178-98(Ref 10), using applied loads of 0.5, 1.0, and 2.0 kg. As-sprayed surface roughness was removed by polishing with 15 μm (800 grit) wet SiC paper prior to scratching. Scratch profiles and depths were characterized using a Hommelwerke (Villingen-Schwenningen, Germany) model Dektak II stylus-tracing profilometer.

3. Results and Discussion

3.1 Powder Characterization

Previous work (Ref 11-13) on composite powders showed that nylon-11 reinforced with nanoscale fumed silica and alumina produced by dry ball-milling had a spheroidal morphology. The ceramic nanoparticles were mechanically embedded into the surface of the nylon-11, forming a hard outer shell approximately 4 μm thick. This outer shell frequently debonded from the parent nylon-11 particles to form composite sheets.

Micron-scale reinforced nylon-11 particles showed varying degrees of ceramic embedding over the 350 nm to 50 μm size range. Backscattered electron and EDS elemental dot map images were used to characterize the degree of incorporation of the reinforcing phase. Figure 1 shows the typical morphology of a nylon-11 particle clad by a layer of 350 nm alumina. The ceramic reinforcement was embedded into the nylon-11, forming a dense surface layer. The polymer particle surface was almost completely covered; with little or no "free" or unbonded alumina observed.

As the reinforcement size was increased, however, the amount of incorporation decreased (Fig. 2). For nylon-11 powders reinforced with 2 μm alumina, for example, the coverage was incomplete. Energy dispersive x-ray analysis showed some nylon-11 visible between alumina particles. Some "free" alumina particles were also observed.

At 5 μm reinforcement size and above, the ceramic shell was observed to become very discontinuous, and significantly more "free" alumina was visible. The coverage became progressively less as the reinforcement particle size approached the size of the nylon-11 particles (Fig. 3). In the case of the 20 μm reinforcement, the majority of the alumina was separated from the polymer, with only limited embedding taking place. For reinforcement particle sizes greater than 20 μm, the ceramic and polymer phases remained completely uncombined. The ball-milled powders were uniformly blended but had not formed composite particles.

The bulk morphology of the micron-scale ceramic reinforced ball-milled powders was similar to that of the nanoreinforced powders described previously; the primary difference being the incompleteness of the ceramic shell and the level of unbound

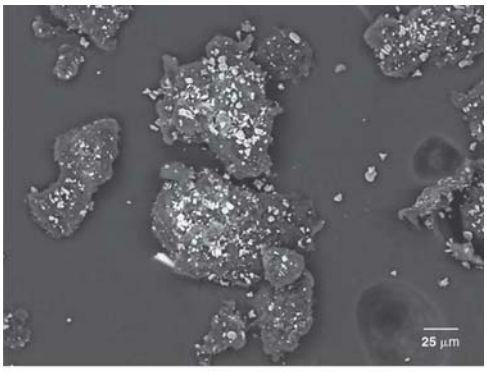

(a)

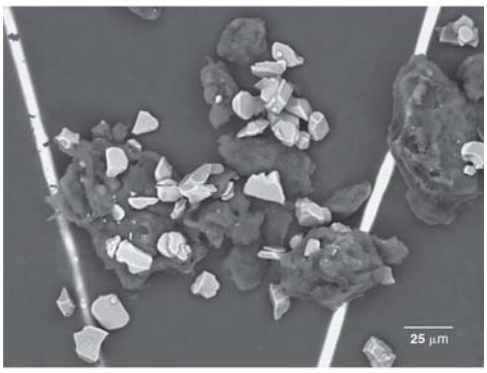

(b)

Fig. 3 SEM images of nylon-11/alumina composite particles: (a) BSE image of nylon-11/5 μm alumina composite particle; (b) BSE of nylon-11/20 μm alumina composite particles

alumina. Figure 4 shows an SEM image of bulk 9 μm reinforced nylon-11. Alumina-rich layers had delaminated from the nylon-11, exposing clean polymer surface. The powders with the largest reinforcement sizes presented difficulties in both ball-milling and HVOF spraying caused by the poor incorporation.

The effectiveness of the silane surface treatment in promoting improved adhesion between the reinforcement and the polymer was characterized by examining polished cross sections of two batches of ball-milled powder particles. One batch was produced from the as-received hydrophilic alumina and the other from the surface-modified ceramic. Figure 5 shows that for powders ball-milled together with the same reinforcement size, the silane-treated ceramic composite exhibited improved adherence and a thicker ceramic shell.

3.2 Coating Microstructure

Coatings were successfully sprayed across the entire nano- and microreinforced range. In general, the coatings were found to be dense and adherent, with some spherical voids/pores approximately 30 μm in diameter observed in the ceramic reinforced coatings. While it has been hypothesized that this porosity may have been caused by water vapor or other gas evolution, the exact origin and understanding of why such voids were absent in HVOF sprayed pure nylon coatings remains under investigation. Figure 6 shows optical micrographs of pure nylon-11 and 7 nm ceramic reinforced coatings, showing the general microstructure and differences in pore morphology. Figure 7 shows SEM-BSE images of a typical microstructure of HVOF sprayed micron-scale alumina reinforced nylon-11 coatings.

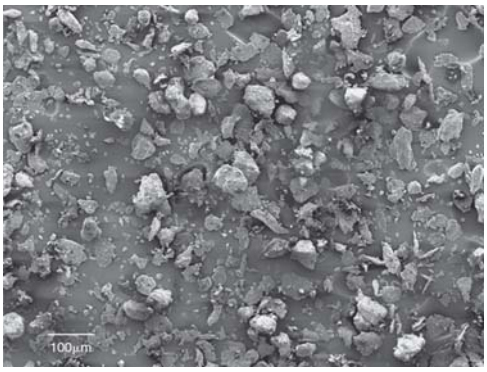

Fig. 4 SEM image of nylon-11/9 μm alumina composite powder particles. The general morphology comprised large nylon-11 particles with alumina-rich surface layers, alumina-rich flakes that debonded from the nylon-11 particles and "free" unbound alumina.

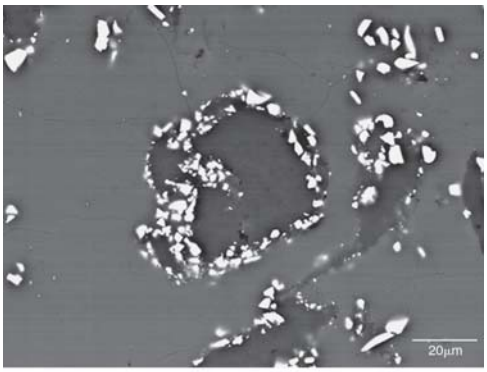

(a)

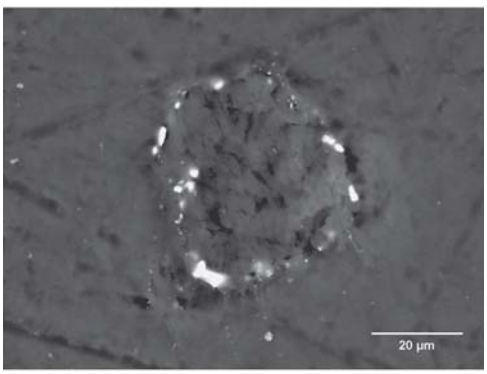

(b)

Fig. 5 Images of composite powder particles: (a) polished cross sections of individual nylon-11/5 μm silane treated (hydrophobic ceramic surface) alumina composite powder particles; (b) BSE image of polished cross sections of individual nylon-11/5 μm untreated (hydrophilic ceramic surface) alumina composite powder particles

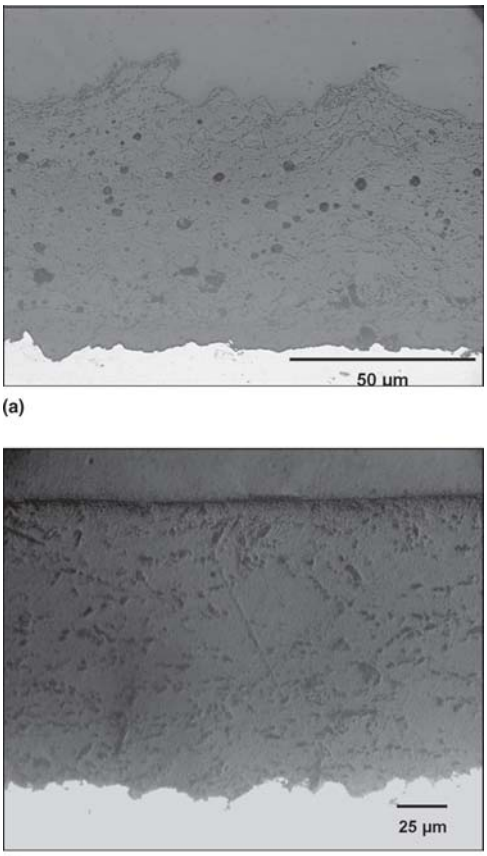

Fig. 6 Optical micrographs of HVOF sprayed coatings: (a) polished cross section of unreinforced nylon-11 coating; (b) nylon-11/7 nm reinforced composite coating

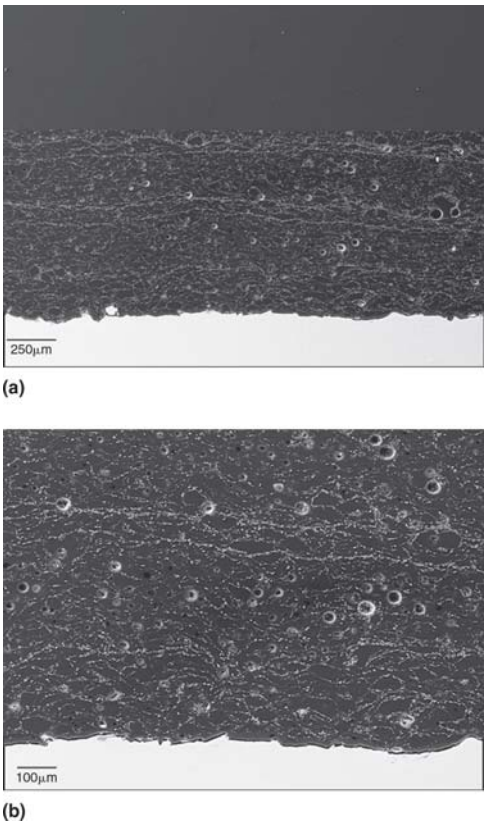

Fig. 7 SEM-BSE images of HVOF sprayed composite coatings: (a) polished cross section of nylon-11/5 µm alumina composite coating; (b) same field as in (a) at higher magnification

The image indicated that the alumina was concentrated at the splat boundaries, but well distributed throughout the polymer matrix in a series of interconnected lamellar sheets. Distinct stratification was visible between passes and where steps overlapped. Chemical microanalysis of the coatings confirmed the distribution of the ceramic phase and that the silane (Silquest) surface treatment withstood the HVOF spray process.

The efficacy of the ball-milling was evident in the microstructures of the coatings. The splat boundaries in coatings with the nanoscale reinforcements were very sharply defined as a result of the dense ceramic-rich shells around the nylon-11 cores of the feedstock powder. As shown in Fig. 8(a) and (b), the 7 and 350 nm ceramic reinforced coatings both exhibited similar microstructures with well-defined splat boundaries and ceramic-rich cells. The powders reinforced with midrange micron-scale ceramic particles exhibited varying levels of incorporation, and consequently the splat boundaries in these coatings appeared broader with gaps where two feedstock particles fused together, as can be observed in the 5 µm ceramic reinforced coating microstructure shown in Fig. 7. As the size of the reinforcement particles increased, the ceramic-rich shells became less complete and the splat boundaries less distinct. As can be seen in Fig. 8(c), coatings reinforced with 20 µm alumina exhibited no distinct splat boundaries or stratification.

3.3 Crystallinity and Crystal Structure

Of the five known crystal structures of nylon-11, only two were observed in the feedstock powders and sprayed coatings. The first was the thermodynamically stable triclinic α form and the second the metastable "smectic" pseudohexagonal δ phase. The α form shows two reflections; the (100) peak at 21° with corresponding *d*-spacing of 0.44 nm and the (010,110) peak at 23.4° with 0.37 nm *d*-spacing. The δ phase showed only one peak (the (100) reflection), which overlapped the (100) α reflection at 21° and had a corresponding *d*-spacing of 0.42 nm. The changes in the amount of δ phase relative to α observed can be calculated from the ratio of the (100) to (010,110) reflection intensities (Ref 14). Figure 9 shows the x-ray diffraction (XRD) pattern for as-received nylon-11 feedstock powder. The powder had a crystallinity of approximately 20%, as reported by the manufacturer (Ref 11). The powder was primarily the α phase but with a significant δ phase contribution. Figure 10 shows the XRD patterns of selected HVOF sprayed coatings, with the reinforcement (alumina and silica) peaks removed for clarity. The pure nylon-11 coatings and nanoscale ceramic reinforced coatings lost the metastable δ phase on spraying while the micron-scale ceramic reinforced coatings retained a low level of the δ structure. The observed loss of δ character is characteristic of a decrease in the spacing of the hydrogen-bonded sheets of nylon-11 chains as the polymer reaches thermodynamic equilibrium (Ref 15). The crystallinity of the sprayed coatings was also ap-

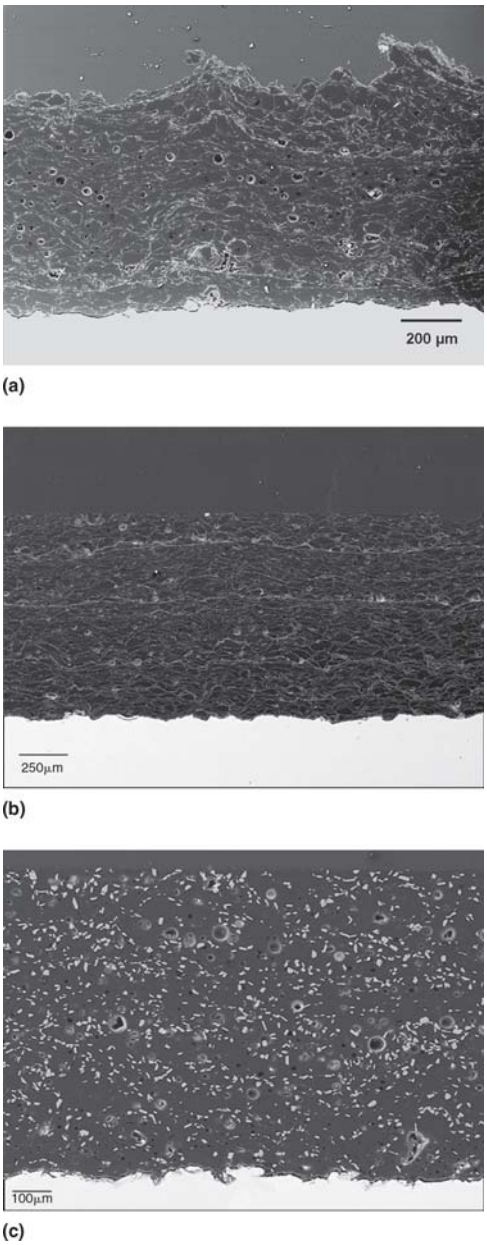

Fig. 8 SEM-BSE images of HVOF sprayed composite coatings: (a) polished cross section of nylon-11/7 nm silica reinforced composite coating; (b) polished cross section of nylon-11/350 nm alumina composite coating; (c) polished cross section of nylon-11/20 µm alumina composite coating

proximately 20%, indicating that the crystallinity of the feedstock powders was maintained during the HVOF spraying, supporting the "semimolten" process described previously.

The δ structure observed in the feedstock powders was most likely an artifact of the fast quenching and cryogrinding process stages of powder production. After spraying, the coatings were allowed to cool relatively slowly (~50 °C/min), allowing time for the δ phase to reorder to the stable α structure. The retention of small amounts of the δ phase in the micron-scale ceramic reinforced coatings may have been caused by differences in thermal properties between the silica and alumina, differences in

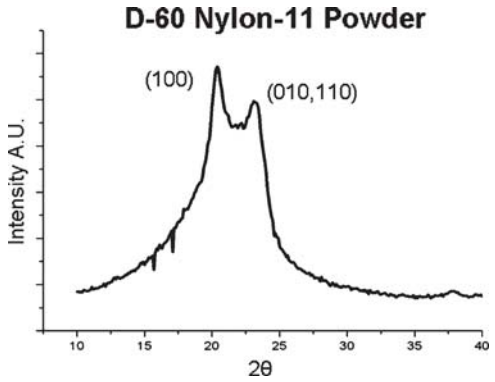

Fig. 9 XRD pattern of as-received nylon-11 D-60 powder

thermal properties of the overall coating caused by the distribution of the ceramic, or by slight variations in the spray parameters. The effect of reinforcement size and HVOF spraying on the crystal structure of the coatings is convoluted, and the effect on the properties of the coatings is currently being investigated.

Figure 10 shows the XRD pattern of an as-sprayed and annealed 5 µm ceramic reinforced coating. The XRD pattern of the coating was measured immediately after spraying, and the coating was then annealed for 24 h at 165 °C (20 °C below the melting point) and measured again. The peaks at 25°, 35° and 40° correspond to the alumina reinforcement and were left in the pattern to scale the nylon peaks. After annealing the crystallinity increased from approximately 20% to approximately 30%, with a large increase in the (110) reflection, indicating an increasing degree of crystallite perfection (Fig. 11). This is the same crystal structure and approximate crystallinity obtained by deep drawing thin nylon-11 films at elevated temperature (Ref 15).

3.4 Scratch Resistance

Figure 12 shows scratch depth as a function of reinforcement size for a 1 kg load. The scratch depth for an HVOF sprayed pure nylon-11 coating was ~60 µm, represented by the horizontal line on the graph. The greatest improvement in scratch resistance relative to pure nylon-11 was 30% observed for a 7 nm alumina reinforced polymer. By contrast, the improvement was only 8% for 20 µm alumina reinforced polymer. Scratch depth decreased with decreasing reinforcement size, as can be seen by following a best fit logarithmic trend line. The 0.5, 1, and 2 kg loadings showed similar trends to that indicated in Fig. 13.

Traditional reinforcement models assume that the mechanical properties depend only on the fraction of bulk replaced by ceramic, a dependence that would scale as a function of the volume of particles, or diameter cubed. Reinforcement might, however, depend on the surface area, that is, proportional to diameter squared, or to the region of polymer volume controlled by the surface and thus related to the number of reinforcement particles. For a range of particle sizes, such as present in a normal or log-normal distribution, a more complex mean, such as a log mean or harmonic mean, may be more appropriate. This work provides a comprehensive experimental evaluation, crossing four orders of magnitude in reinforcement size, and was intended as the first step in exploring this dependence.

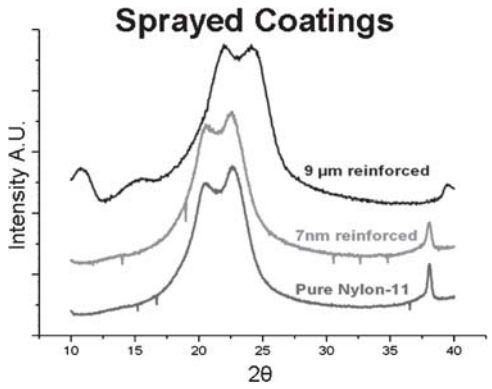

Fig. 10 XRD patterns of HVOF sprayed composite coatings. Upper, 9 μm reinforced; center, 7 nm reinforced; lower, unreinforced nylon-11

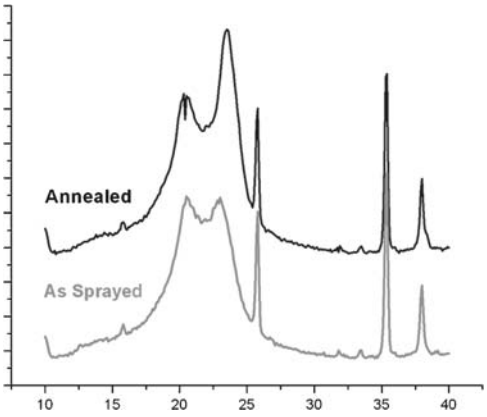

Fig. 11 XRD patterns. Upper, annealed nylon-11/5 μm alumina composite coating; lower, as-sprayed nylon-11/5 μm alumina composite coating

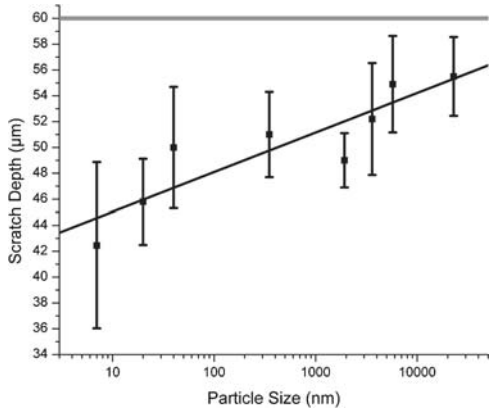

Fig. 12 Scratch depth as a function of reinforcement particle size for a 1 kg load. The horizontal line represents the scratch depth for a pure nylon-11 coating.

Figure 14 shows the differences in scratch scars observed in pure nylon-11 and 7 nm ceramic reinforced coatings. The scratch in the pure polymer coating had very little "pileup" of material

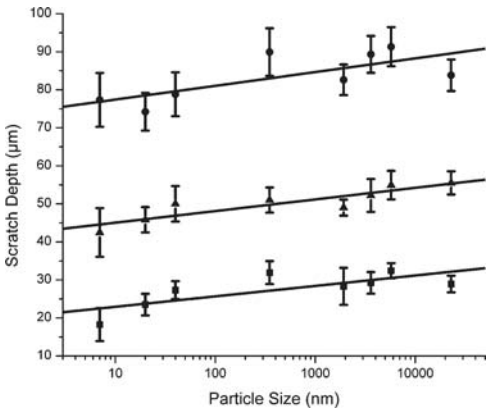

Fig. 13 Scratch depth as a function of reinforcement particle size for 0.5, 1 and 2 kg loadings. The scratch depth followed an identical logarithmic trend for all loadings.

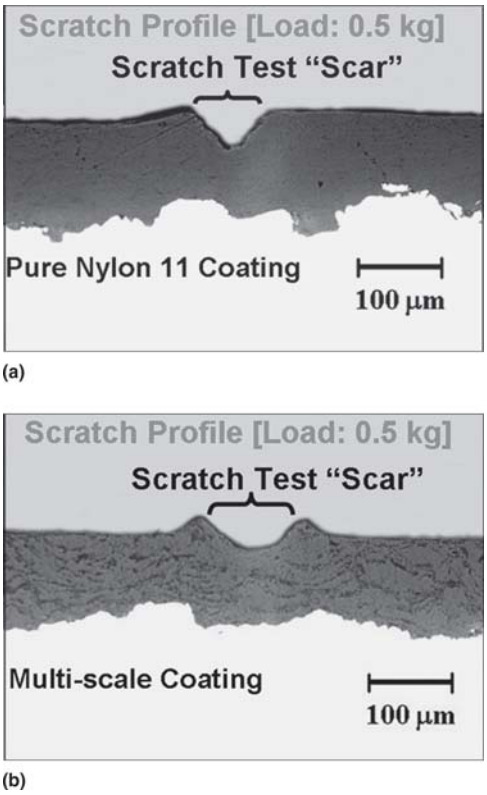

Fig. 14 Optical micrographs of 0.5 kg load scratch "scar" in (a) a pure nylon-11 coating and (b) a nylon-11/7 nm silica reinforced composite coating

on the sides and appeared to have been formed by cutting of the polymer by the scratch tester stylus. The scratch profile of the nanoscale ceramic reinforced coating, however, had a flat "bottom" with a large amount of material pileup at the edges of the scratch, more indicative of a plowing rather than a cutting mechanism. Micron-scale ceramic reinforced coatings exhibited varying degrees of cutting versus plowing. A model of the deformation mechanisms occurring during scratch testing as a

function of reinforcement size is the next step to be undertaken before the actual scratch depth trend can be determined.

The coatings exhibited varying recovery in scratch depth of approximately 25 to 60% over a 14 day period. Pure nylon-11 and coarse micron-scale reinforced coatings exhibited the greatest recovery, while nanoscale reinforced coatings exhibited the least. The scratch behaviors for 35 and 50 μm alumina reinforced coatings were not reported. The scratch tests for these coarse micron-scale reinforced coatings were not repeatable. The inconsistencies could be a result of, for example, interactions between the scratch needle and larger particles with a scale similar to the size of the scratch stylus. These coatings are still under investigation.

4. Summary and Conclusions

Ceramic reinforced nylon-11 matrix coatings have been successfully produced using the HVOF combustion spray process over the full reinforcing particle size range from 7 nm to 50 μm. The microstructures of the coatings appeared dense, coherent, and well adherent to the substrate. The feedstock powders produced by dry ball-milling were characterized, and relationships between powder morphology and coating microstructure and properties established. The effect of reinforcement incorporation into the nylon-11 particles on load transfer mechanisms is currently being investigated. Scratch testing showed up to 30% improvements in scratch resistance for the nanoreinforced coatings when compared with pure nylon-11. XRD analysis reflects differences in crystal structure with respect to reinforcement particle size. The effect of particle size and spray parameters on crystallinity will continue to be explored.

Acknowledgments

The authors would like to thank the National Science Foundation for providing support for this research under collaborative grant number DMI 0209319. The views expressed in this paper do not necessarily reflect those of NSF. The authors also greatly appreciate the assistance and help of Mr. Dustin Doss.

References

1. J. Jordan, K. Jacob, R. Tannenbaum, M. Sharaf, and I. Jusiuk, Experimental Trends in Polymer Nanocomposites, *Mater. Sci. Eng. A,* 2005, **393,** p 1-11
2. M. Sumita, T. Shizuma, K. Miyasaka, and K.J. Ishikawa, Effect of Reducible Properties of Temperature, Rate of Strain and Filler Content on the Tensile Yield Stress of Nylon 6 Composites Filled with Ultrafine Particles, *J. Macromolec. Sci: Phys.,* 1983, **B22**(4), p 601-618
3. P. Messersmith and E. Giannelis, Synthesis and Characterization of Layered Silicate-Epoxy Nanocomposites, *Chem. Mater.,* 1994, **6,** p 1719-1725
4. P. Messersmith and E. Giannelis, Synthesis and Barrier Properties of Poly(ε-caprolactone) Layered Silicate Composites, *J. Polymer Sci. Part A: Polymer Chem.,* 1995, **33,** p 1047-1057
5. K. Yano, A. Usuki, A. Okada, T. Kurauchi, and O. Kamigaito, Synthesis and Properties of Polyimide-Clay Hybrid, *J. Polymer Sci. Part A: Polymer Chem.,* 1993, **31,** p 2493-2498
6. T. Lewis and L. Nielsen, Viscosity of Dispersed and Aggregated Suspension of Spheres, *Trans. Soc. Rheology,* 1968, **12,** p 421-443
7. V. Kumar and L. Erwin, Solvent Assisted Compounding of Highly Filled Thermoplastics, *Proc. Antec'87,* 1987, p 152-156
8. C. Mateus, S. Costil, R. Bolot, and C. Coddet, Ceramic/Fluoropolymer Composite Coatings by Thermal Spraying—A Modification of Surface Properties, *Surf. Coat. Technol.,* 2005, **191,** p 108-118
9. P. Edwin, *Pludeman Silane Coupling Agents,* Plenum, New York, 1982
10. Standard Test Method for Mar Resistance of Organic Coatings, *Annual Book of ASTM Standards,* ASTM, 2002
11. E. Petrovicova, R. Knight, L.S. Schadler, and T.E. Twardowski, Nylon-11/Silica Nanocomposite Coatings Applied by the HVOF Process Part I: Microstructure and Morphology, *J. Appl. Polym. Sci.,* 2000, **77**(8), p 1684-1699
12. E. Petrovicova, R. Knight, L.S. Schadler, and T.E. Twardowski, Nylon-11/Silica Nanocomposite Coatings Applied by the HVOF Process: Part II. Mechanical and Barrier Properties, *J. Appl. Polym. Sci.,* 2000, **78**(13), p 2272-2289
13. V. Gupta, M. Ivosevic, T.E. Twardowski, R.A. Cairncross, and R. Knight, Thermally Sprayed Multi-Scale Polymer/Ceramic Composite Coatings, *Proc. 20th Annual Technical Conference,* American Society for Composites, Philadelphia, PA, Sept 2005, p 48-57
14. Q. Zhang, Z. Mo, and H. Zhang, S. Liu, and S.Z.D. Cheng, Crystal Transitions of Nylon-11 under Drawing and Annealing, *Polymers,* 2001, **42**(13), p 5543-5547
15. K. Chen, B. Newman, J. Scheinbeim, and K. Pae, High Pressure Melting and Crystallization of Nylon-11, *J. Mater. Sci.,* 1985, **20,** p 1753-1762